

Transmission of heat modes across a potential barrier

Amir Rosenblatt^{1,†}, Fabien Lafont^{1,†}, Ivan Levkivskyi², Ron Sabo¹,
Itamar Gurman¹, Daniel Banitt¹, Moty Heiblum¹ and Vladimir Umansky¹
¹*Braun Center for Submicron Research, Dept. of Condensed Matter physics,
Weizmann Institute of Science, Rehovot 76100, Israel and*

²*Institute of Ecology and Evolution, University of Bern, CH-3012 Bern, Switzerland*

([†]These authors contributed equally to this work)*

ABSTRACT

Controlling the transmission of electrical current using a quantum point contact constriction paved a way to a large variety of experiments in mesoscopic physics. The increasing interest in heat transfer in such systems fosters questions about possible manipulations of quantum heat modes that do not carry net charge (neutral modes). Here, we study the transmission of upstream neutral modes through a quantum point contact in fractional hole-conjugate quantum Hall states. Employing two different measurement techniques, we were able to render the relative spatial distribution of these chargeless modes with their charged counterparts. In these states, which were found to harbor more than one downstream charge mode, the upstream neutral modes are found to flow with the inner charge mode - as theoretically predicted. These results unveil a universal upstream heat current structure and open the path for more complex engineering of heat flows and cooling mechanisms in quantum nano-electronic devices.

INTRODUCTION

The intimate link between heat current, entropy flow and therefore information transfer [1, 2], triggered recent interest in thermoelectric effects occurring at the nanoscale, such as measurements of the quantum limit of heat flow of a single quantum mode [3–6], heat Coulomb blockade of a ballistic channel [7] or quantum limited efficiency of heat engines and refrigerators [8, 9]. One main experimental obstacle in measuring thermal effects is to decouple the charge from heat currents. Such separation is made easier in the fractional quantum Hall effect (FQHE) [10], since, at least in hole-conjugate states (say, $1/2 < \nu < 1$), chargeless heat modes propagate with an opposite chirality (upstream) to that of the charge modes [11–13]. Theoretically, while Laughlin wave function [14] has a great success

in describing various aspects of the FQHE at filling factors $\nu = 1/m$, with odd m , the structure of hole-conjugate filling fractions, such as $\nu = 2/3$ and $\nu = 3/5$, is still not clear. Two edge-model structures had been proposed for the most studied $\nu = 2/3$ state, the first considers this state as a charge conjugate of the $\nu = 1/3$ state; namely, a $\nu = 1/3$ hole Landau level (LL) in the completely filled $\nu = 1$ electronic LL form a Laughlin condensate with $\nu = 1/3$ [15, 16]. The second, considers it as a $\nu = 1$ type condensate of fractional $e^* = 1/3$ quasiparticles on top of the $\nu = 1/3$ state [17, 18]. Interestingly, recent experiments with a softly defined edge potential (induced by a gate) showed that the structure of the edge charge modes at filling factors $\nu = 2/3$ (and similarly at $\nu = 3/5$) is in fact composed of two spatially separated charge modes [19], that would suggest the second point of view to be more appropriate. Furthermore, topological arguments require to have a conserved total number of net modes, therefore predicting two upstream neutral modes at $\nu = 2/3$, and three at $\nu = 3/5$.

Here, we fully characterize the transmission of the downstream charge modes and the upstream neutral modes through a potential barrier, imposed by a quantum point contact (QPC). We show their relative spatial distribution and heat power carried by the neutral modes. Using the same device, we shed more light on the interplay between charge and neutral modes impinging on a QPC by distinguishing thermal fluctuations from shot noise.

RESULTS

Transmission of neutral modes across a QPC

The experimental setup, designed to map the transmission of neutral modes through a QPC constriction, is presented in Figs. 1a, 1c, 1e. The QPC (on the right) partitions either the charge mode emitted from S2 (Fig. 1a), or the neutral modes excited by the hot spot at the back of contact H (Figs. 1c & 1e). In the latter case, two methods were employed to convert the energy carried by the neutral modes to a measurable charge current. The first utilized a quantum dot (QD, on the left) to convert a temperature gradient to a net thermoelectric current [20–

* correspondence should be addressed to: lafont.fabien@gmail.com

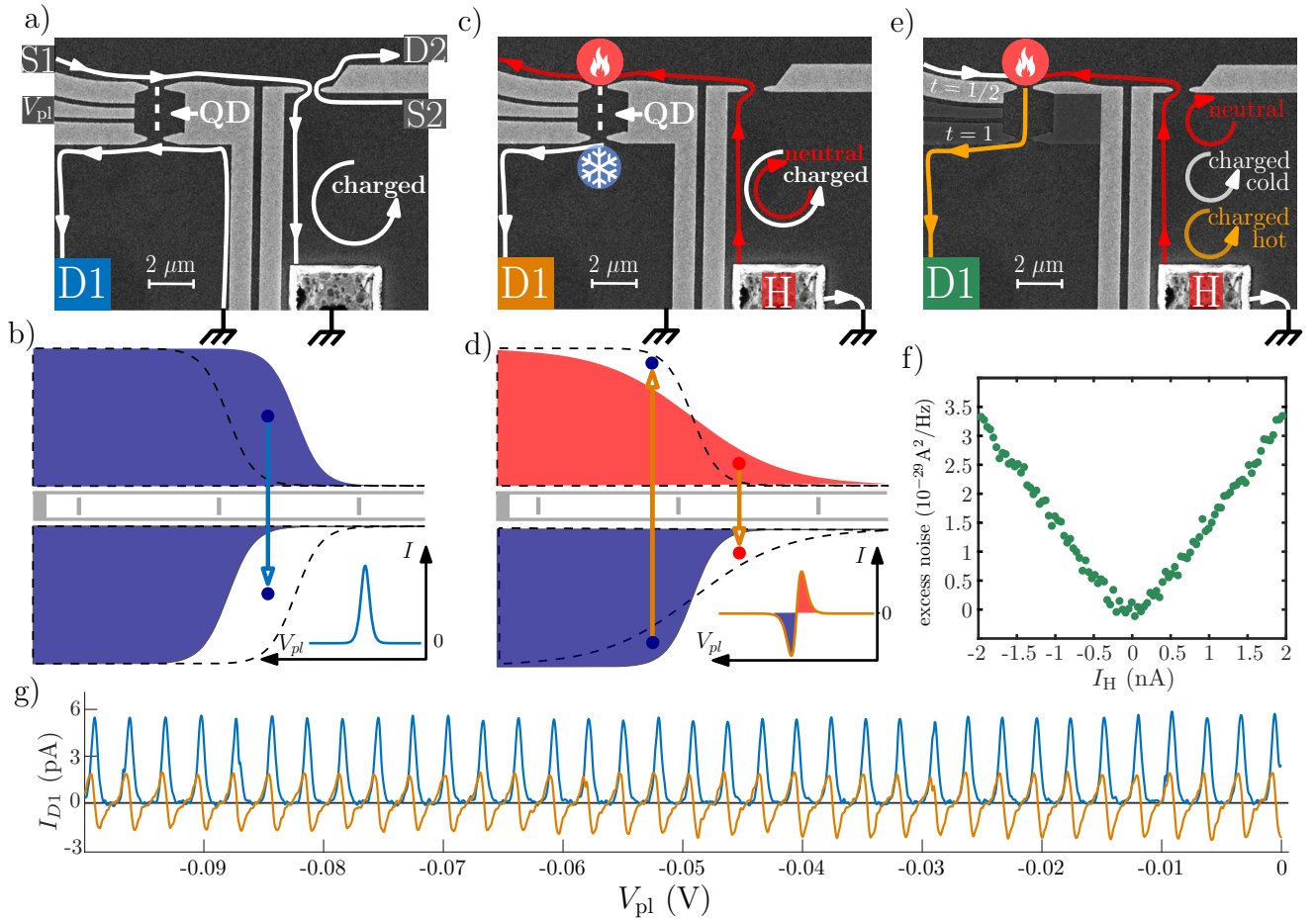


Figure 1. Description of the experimental device and methods: **a)** Scanning electron microscope (SEM) image of the device. In this configuration the current is sourced from S1, reaching to the quantum dot (QD). Sweeping the plunger gate voltage results in a succession of Coulomb peaks as shown by the blue curve on **g)**. **b)** Schematic of the equilibrium distribution on each side of the QD. When the plunger gate is tuned, electron can tunnel into the dot from the high occupation number region to the lower one, creating a positive current measured at D1. **c)** Neutral mode heat detection configuration: The current sourced in H is directed to the ground and plays no part in the experiment. A hot spot present at the upstream side of contact H excites the neutral heat modes flowing upstream towards the QD, creating a thermal gradient across the QD. The produced thermoelectric current then flows to D1. **d)** Sketch of the equilibrium distribution on both side of the dot in the case depicted in **c)**. In this case the tunneling direction will depend if an energy level of the QD is placed below or above the center of the distribution. This induces an alternating current when the plunger gate is tuned. **e)** Noise measurement configuration: Here the input QPC of the QD is set to half transmission while the second one is fully open. This turns the QD into an effective single QPC device. The heat carried by the neutral modes increase the electron temperature at the input QPC of the dot, which increases the Johnson-Nyquist noise, measured at D1. **f)** Excess noise measured at D1 as function of current injected in H, as described in **e)**. **g)** Measurement corresponding to the configuration **a)** in blue and **c)** in orange.

24] as sketched in Fig. 1c. With the thermal distribution at the input of the QD being hotter than at the output, scanning the energy level of the QD leads to a net thermoelectric current through the QD with an alternating polarity (see Fig. 1d and Fig. 1g, and experimental details in Methods Section). The second approach used excess noise measurements, resulting from the upstream heat current impinging on a QPC (Fig. 1e) [11, 25, 26]. Here, the input-QPC of the QD was tuned to transmission half while the output-QPC was fully open; therefore turning the QD

to a single QPC. The impinging neutral mode increases the electron temperature at the QPC and accordingly the Johnson-Nyquist noise measured at D1 (Fig. 1f).

The thermopower of a QD, subjected to such a thermal gradient, was studied both theoretically and experimentally [21–23, 27]. On the theoretical side, one needs to obtain the thermoelectric current while considering a specific model of the edge modes structure (see below). On the experimental side, we can directly relate the thermoelectric current to the heat current carried by the transmit-

ted neutral modes (Fig. 2a). Since half of the injected power into contact H, $P_H = 1/2 \times IV$, is dissipated on the hot spot at the back of the ohmic contact H, it is proportional to the heat current (more details in sup. material), $P \propto (T_1^2 - T_0^2) \times \pi^2 k_B^2 / 6h$, carried away by the neutral modes which allows us to map the thermoelectric current to the heat flow [3, 4]. Utilizing this correspondence, the spatial distribution of the neutral modes can be ascertained by measuring their transmission through a QPC constriction. Applying constant power (~ 20 fW) to contact H and measuring the thermoelectric (TE) current across the QD as we gradually pinch the right-QPC (see details in Measurement technique), we find the evolution of heat current carried by the neutral modes (“neutral transmission”), that we present on Fig. 2c (blue curve) together with the conductance of the QPC (black curve). The neutral-transmission was extracted by taking the corresponding power for a given measured TE current from the mapping in Fig. 2a (blue curve); normalized to a fully open right-QPC. A second measurement, using the noise thermometry technique described above was used to validate the neutral transmission. The results are presented on Fig. 2c-red curve, where we plot the evolution of $T_1^2 - T_0^2$ (which is proportional to the heat current carried by the neutral modes, see sup. material), where T_1 is measured and $T_0 = 30$ mK is the base fridge temperature. It is clear from Fig. 2c that the two methods led to consistent results. Comparing the neutral transmission with the one of the charge modes, one notices that $\sim 80\%$ of the neutral mode power is reflected when the inner charge mode, with conductance of $e^2/3h$, is reflected (at the beginning of the conductance plateau, around $V_{QPC} = -0.4$ V), showing that most of the upstream heat flow is ‘attached’ to the inner charge mode. A very similar result was obtained for $\nu = 3/5$ with strong correlation between the reflection of the inner charge mode and the reflection of the heat modes (Fig. 2e).

Theoretical Model

We now compare our experimental results to a theoretical model of the $\nu = 2/3$ state. The first model for such state was developed by MacDonald [15], that predicted two counter-propagating charged edge modes with respective conductance e^2/h flowing downstream and $e^2/3h$ flowing upstream. Due to the absence of any experimental evidence of upstream current [28], Kane, Fisher and Polchinski [16, 29] introduced scattering between the above mentioned channels leading to a single downstream charge mode with conductance $2e^2/3h$ and an upstream neutral mode. Later, Meir *et al.* [17, 18] refined this model for a soft edge potential (which is the case for gate-defined edge, like presently) and proposed an edge modes picture presented on Fig. 2b. A smooth confining potential in-

duces a non-trivial density variation near the edge: Starting from the bulk, the local filling factor goes from $2/3$ to 1 creating an upstream charge mode of conductance $e^2/3h$. The subsequent filling factor drop goes from unity to 0 and therefore creates a charge mode going downstream with an associated conductance equal to e^2/h . Finally, an extra density hump reaching $\nu = 1/3$ creates a pair of $G = e^2/3h$ counter propagating channels. Taking into account interactions and scattering between the channels leads to the presence of a decoupled channel with conductance $e^2/3h$ of width ξ_0 close to the edge, flowing next to an inner, wider channel of width ξ , also with conductance $e^2/3h$ accompanied by two neutral modes flowing upstream. Note, that there are several alternative pictures of QH states at filling factors $2/3$ and $3/5$ both with and without neutral upstream edge modes (see, e.g., [30]). Moreover, edge reconstruction phenomena [31, 32] (e.g. additional humps in the density) can affect both the microscopic and effective behavior of edge states. Therefore, we focus our discussion on the simplest effective model of edge states that is less sensitive to the details of experimental situation. The theoretical model presented here utilizes the “Meir *et al.*” edge structure where couplings between channels leads to different excitation. The outer edge mode is completely decoupled from all other channels, while the inner channel gives rise to excitations, each characterized by a charge e^* and a scaling dimension Δ (see details in Supplementary note 4), which allow us to calculate the TE current through a single energy level ϵ_0 of the QD for this particular edge state picture and for dominant excitation with $e^* = 1/3$ and $\Delta = 1$ [33]:

$$I_{TE} \propto [f_{out}(T_{out}, \epsilon_0) f_{in}(T_{in}, -\epsilon_0) - f_{in}(T_{in}, \epsilon_0) f_{out}(T_{out}, -\epsilon_0)] \quad (1)$$

where f_{out} , f_{in} , T_{out} , T_{in} are the occupation numbers and temperatures corresponding to the Input and Output side of the quantum dot. Considering that the two upstream modes originate from a hot reservoir at temperature T_1 and the downstream ones at temperature T_0 , it is possible to express the QD’s input/output occupation number as,

$$f_{in}(\epsilon_0) = \int dt e^{i\epsilon_0 t} \left[\frac{T_0}{\sinh(\pi T_0(t - i\eta))} \right]^{\delta_0} \left[\frac{T_1}{\sinh(\pi T_1(t - i\eta))} \right]^{\delta_1} \quad (2)$$

with $\delta_0 = 1/3$, $\delta_1 = 2/3$, $\Delta = \delta_0 + \delta_1 = 1$ and

$$f_{out}(\epsilon_0) = \int dt e^{i\epsilon_0 t} \frac{T_0}{\sinh(\pi T_0(t - i\eta))} = \frac{1}{e^{\epsilon_0/T_0} + 1} \quad (3)$$

Inserting Eqs. (2) & (3) in Eq. (1) one can calculate the evolution of the TE current in a QD with a single energy level for this particular edge modes picture (see Supplementary note 4). The results either using effective temperature approximation or exact numeric integration are plotted in Fig. 2a. The good agreement between the theoretical and experimental results strengthen the validity of an edge picture that consists of two charge modes accompanied by two upstream neutral modes. Using the same theoretical

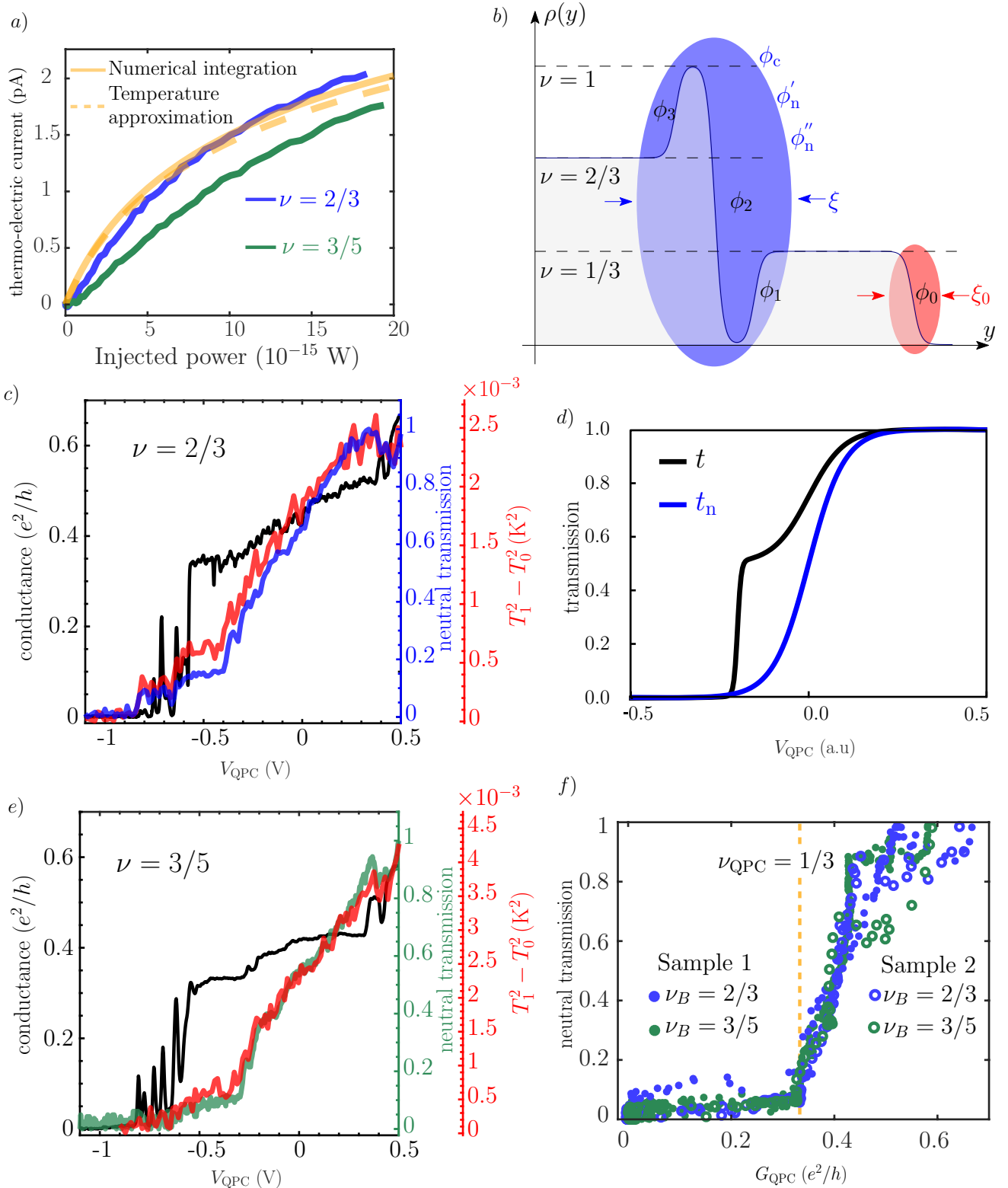


Figure 2. **Transmission of neutral modes:** **a)** Evolution of the thermo-electric current as function of the Joule power applied on H at $\nu = 2/3$ (blue curve) and at $\nu = 3/5$ (green curve). Theoretical prediction of the thermo-electric current through the QD, orange dashed curve shows effective temperature approximation, orange solid curve shows result of exact numeric integration. **b)** Theoretical model of the edge structure of the $\nu = 2/3$ state. Before equilibration four charge modes $\phi_{0,1,2,3}$ are considered with respective velocity set by $\partial\rho(y)/\partial y$. After renormalization the system consists of two downstream charge modes of different width ξ and ξ_0 and two upstream neutral modes attached to the inner mode. **c)** black curve-left axis: Conductance at the QPC constriction as function of the QPC split gate voltage at $\nu = 2/3$, blue curve-right blue axis: Evolution of the neutral transmission as function of the QPC split gate voltage. Red curve-red axis: evolution of the excess noise measured at D1 as function of the QPC split gate voltage. **d)** Theoretical charge and neutral transmission. **e)** Similar to c) at filling factor $\nu = 3/5$. **f)** Neutral transmission as function of the conductance in the QPC constriction for the bulk filling factors $\nu_B = 2/3$ and $\nu_B = 3/5$. The plain and open symbols designate two different samples.

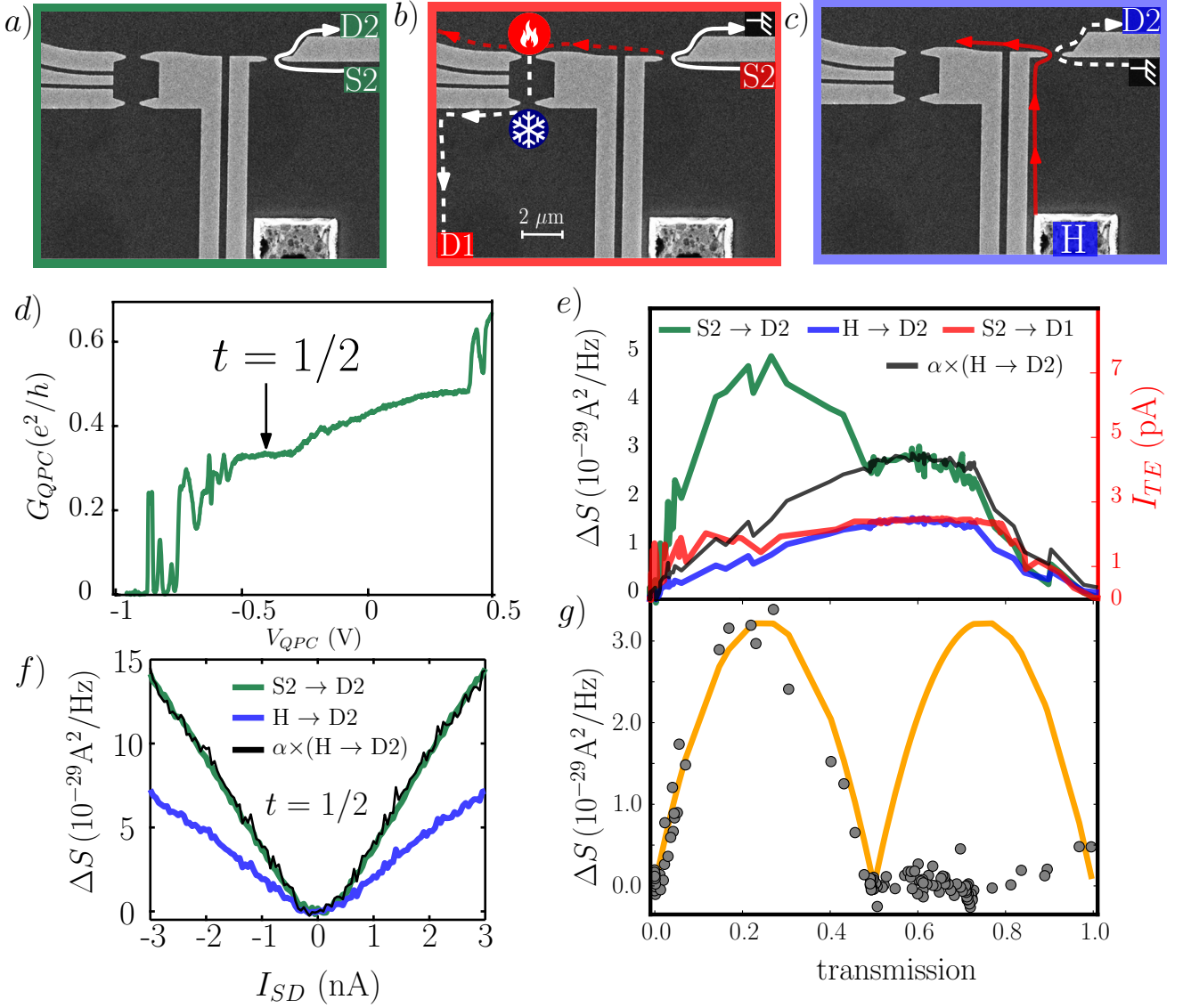


Figure 3. **Noise measurements:** **a)** Sketch of noise measurement at D2 when sourcing charge current from S2 **b)** Sketch of thermoelectric measurement at D1 when sourcing from S2, the impinging current generates heat carried upstream by the neutral modes and converted to thermoelectric current at the QD. **c)** Sketch of noise measurement at D2 when sourcing from H, the upstream neutral modes excited at the hot spot increase the Johnson–Nyquist noise measured at D2 **d)** Conductance of the QPC as function of the split gate voltage. **e)** Green: Current fluctuations measured at D2 when sourcing from S2 as function of the transmission of the QPC. Blue: Current fluctuations measured at D2 when sourcing from H. black: Same as blue multiplied by a scaling factor $\alpha = 2$. Red: Thermoelectric current measured at D1 when sourcing from S2. **f)** Excess noise measured at D2 as function of the current at transmission half when sourcing from S2 (green) or H (blue). The black curve represents the noise from H to D2 (blue curve) multiplied by the scaling factor $\alpha = 2$. **g)** Grey dots: Shot noise contribution $N_{SN} = N_{tot} - \alpha N_{th} = N_{S2 \rightarrow D2} - \alpha N_{H \rightarrow D2}$. Orange curve: expected shot noise from 2 separated ballistic charge channels.

picture, we have modeled the neutral and charge transmissions through the QPC constriction using a quasi-classical approximation [34]:

$$t_i(V) = 1 / \left(1 + e^{(V-V_i)/\delta V_i} \right) \quad (4)$$

where $i = \text{inner, outer}$. In our model there are two modes that are spatially separated, therefore they will be centered

around different gate voltage V_i of the split-gate QPC, and with different width corresponding to δV_i . The total charge transmission $t_{\text{charge}}(V) = (t_{\text{inner}}(V) + t_{\text{outer}}(V)) / 2$ is plotted in Fig.2d together with the neutral transmission, $t_{\text{neutral}}(V) = t_{\text{inner}}(V)$, where both the neutral modes are located near the inner charge mode. As visible on Fig.2d, this simple model is able to qualitatively explain the transmission of the neutral modes; and in particular the observed

vanishing of the neutral transmission when the conductance reaches $G_{\text{QPC}} = 1/3$. To compare in more details the measured transmission of the neutral modes in the two bulk fractions, $\nu_B = 2/3$ and $\nu_B = 3/5$, we have plotted each one as function of the conductance of the QPC constriction G_{QPC} (Fig.2f). Surprisingly, they present a nearly identical behavior, which strongly suggests that, at least for these two hole-conjugate states, the transmission of the neutral modes is dictated by the conductance of the QPC and is poorly dependent on the bulk filling factor. We have plotted on the same figure (open symbols) the results of another similar sample (presented in Supplementary note 1). It is clear that the curves present an overlap on a large G_{QPC} region which indicates that the structure of the neutral modes is universal and do not depend on the bulk state as well as the particular mobility or disorder in the QPC constriction.

Excess noise subtraction

Noise measurements reveal even more about energy exchange mechanisms between the charge and neutral modes. We first start from the configuration presented on Fig.3a, where we measure excess-noise in D2 when sourcing DC current from S2. As shown on Figs. 3e & 3f (green curves) and reported previously [25, 26, 35, 36], the noise remain finite when the QPC is tuned to the conductance plateau at $t_{\text{QPC}} = 1/2$ with $G_{\text{QPC}} = e^2/3h$ (Fig. 3d). This finite noise is even more puzzling since in recent experiment [19] it was shown that two spatially separated channels are present, excluding the presence of conventional shot noise at such transmission. Taking advantage of this device we were able to show that a thermal contribution is added to the shot noise. In order to distinguish between the thermal noise and the partition noise of the quasiparticles (shot noise), the TE current in the QD was measured as function of the right-QPC, but this time the current was sourced in S2 (Fig. 3b). The finite measured thermoelectric current presented on Fig. 3e (red curve) is a clear signature of heat dissipation occurring at the right-QPC constriction where the charge modes exchange energy with the neutral mode. Similarly, exciting neutral modes using contact H as shown in Fig. 3c, increases locally the electronic temperature at the QPC – as discussed before (Fig. 3f, blue curve). Indeed, a similar dependence on the right-QPC transmission, in both measurements, is observed in Fig. 3e. Subsequently, it is interesting to exclude the thermal contribution from the total excess noise measured at D2 when sourcing from S2 and be left with the shot-noise contribution solely. In order to do that, we subtracted the thermal noise N_{th} multiplied by a constant α , that characterizes the neutral mode decay, from the total noise N_{tot} . The constant α was chosen such that the

shot noise contribution at half-transmission would be zero - as expected from a full transmission of one channel and a full reflection of the second. The result of this subtraction $N_{\text{sn}} = N_{\text{tot}} - \alpha N_{th}$ is plotted on Fig. 3g together with the expected excess noise (orange curve) for two charged channels giving a “double hump” shape (due to the $t(1-t)$ dependence of the noise of each channel). The shot noise N_{SN} follows the expected behavior in the range $0 - 0.5$ of total QPC transmission, but then collapses to zero in all the region above half transmission. This would imply that the measured noise when the inner mode is being partitioned results solely from thermal fluctuations - consistent with the neutral modes being attached to the inner channel. This would furthermore indicate that, the outer mode can be partitioned like a ballistic channel while the inner one exhibits dissipation. More experimental and theoretical studies of this excess noise are required to have a full picture of such state.

DISCUSSION

Via studying the transmission of neutral modes through a QPC constriction at hole conjugate states, $\nu = 2/3$ and $\nu = 3/5$ we showed that this structure is consistent with the presence of two upstream neutral modes attached to the downstream inner charge mode; being in agreement with the proposed model by Meir [17, 18]. Moreover, this transmission of the neutral modes through a barrier formed by a QPC constriction is governed by its conductance and does not depend on the bulk-filling factor. This suggests a universality of the neutral modes morphology, which should guide future theoretical models describing them and their interplay with the charge modes. More generally, these results mark a new step in the understanding of heat transport in the FQHE regime as well as for possible future implementation of controlled engineering of heat currents on nanoscale electronic devices.

METHODS

Sample fabrication

The samples were fabricated in GaAs–AlGaAs heterostructures, embedding a 2DEG, with an areal density of $(1.2-2.5) \times 10^{11} \text{cm}^{-2}$ and a 4.2K “dark” mobility $(3.9-5.1) \times 10^6 \text{cm}^2 \text{V}^{-1} \text{s}^{-1}$, 70–116 nm below the surface. The different gates were defined with electron beam lithography, followed by deposition of Ti/Au. Ohmic contacts were made from annealed Au/Ge/Ni. The sample was cooled to 30 mK in a dilution refrigerator.

Conductance measurements were done by applying an a.c. signal with $\sim 1\mu\text{V}$ r.m.s. excitation around 1.3 MHz in the relevant source. The drain voltage was filtered using an LC resonant circuit and amplified by homemade voltage preamplifier (cooled to 1 K) followed by a room-temperature amplifier (NF SA-220F5).

For the thermoelectric current measurement, an alternating voltage V_H at frequency $f \approx 650$ kHz was applied to contact H, giving rise to an upstream neutral modes with temperature proportional to $|V_H|$, producing a series of harmonics starting at $2f$. The heat reaching the upper side of the QD generates an alternating thermoelectric current flowing to drain D1. The signal is then filtered using an LC circuit with a resonant frequency at $2f = 1.3$ MHz amplified by a home-made voltage cold amplifier followed by a room-temperature amplifier, and finally reaching a lock-in amplifier set to measure at frequency $2f$. The thermoelectric current was measured by sweeping the plunger gate for a given V_H amplitude by averaging the peak-to-peak voltage of more than 20 consecutive oscillations. The QD is in the metallic regime $\Delta E \ll k_B T \ll e^2/C$ where the temperature is above the level spacing ΔE and below the charging energy $e^2/k_B C = 290$ mK (see Coulomb diamond measurement in Supplementary note 3).

The data that support the plots within this paper and other findings of this study are available from the corresponding author upon request.

Acknowledgments

A.R and F.L acknowledge Robert Whitney, Ady Stern, Yuval Gefen, Jinhong Park and Kyrlyo Snizhko for fruitful discussions. M.H. acknowledges the partial support of the Minerva Foundation, grant no. 711752, the German Israeli Foundation (GIF), grant no. I-1241- 303.10/2014, the Israeli Science Foundation, grant no. ISF- 459/16 , and the European Research Council under the European Community's Seventh Framework Program (FP7/2007-2013)/ERC Grant agreement No. 339070.

Author contributions

A.R., F.L., R.S., I.G., and M.H. designed the experiment, A.R., F.L., R.S., I.G., D.B. performed the measurements, A.R., F.L., R.S., I.G., D.B. and M.H. did the analysis, I.L. developed the theoretical model. A.R., F.L., I.L. and M.H. wrote the paper. V.U. grew the 2DEG.

Competing Financial Interest

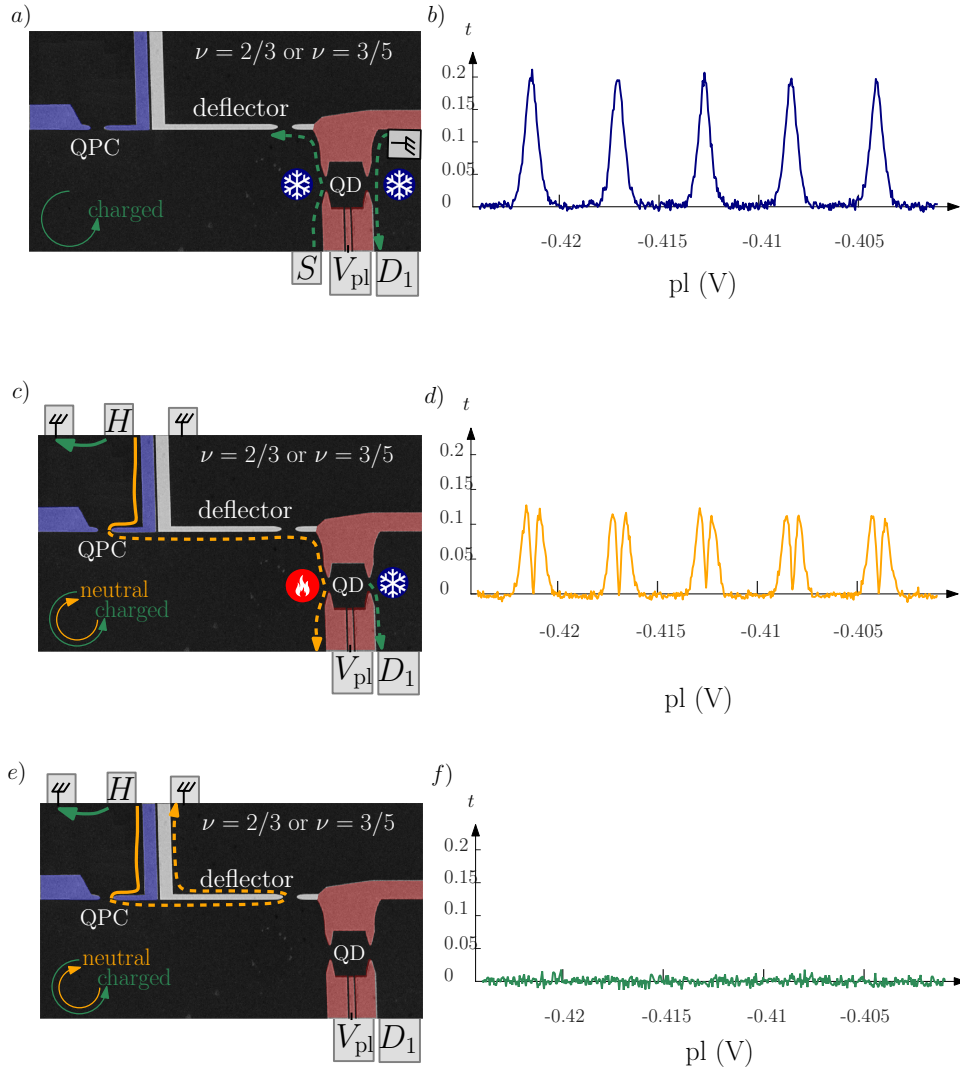
The authors declare no competing financial interests.

-
- [1] Pendry, J. B. Quantum limits to the flow of information and entropy. *Journal of Physics A: Mathematical and General* **16**, 2161–2171 (1983).
- [2] Sivan, U. & Imry, Y. Multichannel Landauer formula for thermoelectric transport with application to thermopower near the mobility edge. *Physical Review B* **33**, 551–558 (1986).
- [3] Jezouin, S. *et al.* Quantum Limit of Heat Flow Across a Single Electronic Channel. *Science* **342** (2013).
- [4] Banerjee, M. *et al.* Observed quantization of anyonic heat flow. *Nature* **545**, 75–79 (2017).
- [5] Banerjee, M. *et al.* Observation of half-integer thermal Hall conductance. *cond-mat.mes-hall* .
- [6] Roukes, M. L., Schwab, K., Henriksen, E. A. & Worlock, J. M. Measurement of the quantum of thermal conductance. *Nature* **404**, 974–977 (2000).
- [7] Sivre, E. *et al.* Heat Coulomb blockade of one ballistic channel. *Nature Physics* (2017).
- [8] Muhonen, J. T., Meschke, M. & Pekola, J. P. Micrometre-scale refrigerators. *Reports on Progress in Physics* **75**, 46501 (2012).
- [9] Whitney, R. S. Most efficient quantum thermoelectric at finite power output. *Physical Review Letters* **112**, 130601 (2014).
- [10] Tsui, D. C., Stormer, H. L. & Gossard, A. C. Two-Dimensional Magnetotransport in the Extreme Quantum Limit. *Physical Review Letters* **48**, 1559–1562 (1982).
- [11] Bid, A. *et al.* Observation of neutral modes in the fractional quantum Hall regime. *Nature* **466**, 585–90 (2010).
- [12] Altimiras, C. *et al.* Chargeless Heat Transport in the Fractional Quantum Hall Regime. *Physical Review Letters* .
- [13] Venkatachalam, V., Hart, S., Pfeiffer, L., West, K. & Yacoby, A. Local thermometry of neutral modes on the quantum Hall edge. *Nature Physics* **8**, 676–681 (2012).
- [14] Laughlin, R. B. Anomalous Quantum Hall Effect: An Incompressible Quantum Fluid with Fractionally Charged Excitations. *Physical Review Letters* **50**, 1395–1398 (1983).
- [15] MacDonald, A. H. Edge states in the fractional-quantum-Hall-effect regime. *Physical Review Letters* **64**, 220–223 (1990).

- [16] Kane, C. L., Fisher, M. P. A. & Polchinski, J. Randomness at the edge: Theory of quantum Hall transport at filling $\nu=2/3$. *Physical Review Letters* **72**, 4129–4132 (1994).
- [17] Meir, Y. Composite edge states in the $\nu=2/3$ fractional quantum Hall regime. *Physical Review Letters* **72**, 2624–2627 (1994).
- [18] Wang, J., Meir, Y. & Gefen, Y. Edge reconstruction in the $\nu=2/3$ fractional quantum Hall state. *Physical review letters* **111**, 246803 (2013).
- [19] Sabo, R. *et al.* Edge reconstruction in fractional quantum Hall states. *Nature Physics* (2017).
- [20] Beenakker, C. W. J. & Staring, A. A. M. Theory of the thermopower of a quantum dot. *Physical Review B* **46**, 9667–9676 (1992).
- [21] Staring, A. A. M. *et al.* Coulomb-Blockade Oscillations in the Thermopower of a Quantum Dot. *Europhysics Letters (EPL)* **22**, 57–62 (1993).
- [22] Viola, G., Das, S., Grosfeld, E. & Stern, A. Thermoelectric probe for neutral edge modes in the fractional quantum hall regime. *Physical Review Letters* **109**, 146801 (2012).
- [23] Gurman, I., Sabo, R., Heiblum, M., Umansky, V. & Mahalu, D. Extracting net current from an upstream neutral mode in the fractional quantum Hall regime. *Nature communications* **3**, 1289 (2012).
- [24] Altimiras, C. *et al.* Non-equilibrium edge-channel spectroscopy in the integer quantum Hall regime. *Nature Physics* **6**, 34–39 (2010).
- [25] Gross, Y., Dolev, M., Heiblum, M., Umansky, V. & Mahalu, D. Upstream Neutral Modes in the Fractional Quantum Hall Effect Regime: Heat Waves or Coherent Dipoles. *Physical Review Letters* **108**, 226801 (2012).
- [26] Inoue, H. *et al.* Charge Fractionalization in the Integer Quantum Hall Effect. *Physical Review Letters* **112**, 166801 (2014).
- [27] Beenakker, C. W. J. Edge channels for the fractional quantum Hall effect. *Physical Review Letters* **64**, 216–219 (1990).
- [28] Ashoori, R. C., Stormer, H. L., Pfeiffer, L. N., Baldwin, K. W. & West, K. Edge magnetoplasmons in the time domain. *Physical Review B* **45**, 3894–3897 (1992).
- [29] Kane, C. L. & Fisher, M. P. A. Impurity scattering and transport of fractional quantum Hall edge states. *Physical Review B* **51**, 13449–13466 (1995).
- [30] Wu, Y.-H., Sreejith, G. J. & Jain, J. K. Microscopic study of edge excitations of spin-polarized and spin-unpolarized $\nu = 2 / 3$ fractional quantum Hall effect. *Physical Review B* **86**, 115127 (2012).
- [31] Chklovskii, D. B., Shklovskii, B. I. & Glazman, L. I. Electrostatics of edge channels. *Physical Review B* **46**, 4026–4034 (1992).
- [32] Aleiner, I. L. & Glazman, L. I. Novel edge excitations of two-dimensional electron liquid in a magnetic field. *Physical Review Letters* **72**, 2935–2938 (1994).
- [33] Levkivskiy, I. P., Boyarsky, A., Fröhlich, J. & Sukhorukov, E. V. Mach-Zehnder interferometry of fractional quantum Hall edge states. *Physical Review B* **80**, 045319 (2009).
- [34] Buttiker, M. Quantized transmission of a saddle-point constriction. *Physical Review B* **41**, 7906–7909 (1990).
- [35] Saminadayar, L., Glattli, D. C., Jin, Y. & Etienne, B. Observation of the $e/3$ Fractionally Charged Laughlin Quasiparticle. *Physical Review Letters* **79**, 2526–2529 (1997).
- [36] Bid, A., Ofek, N., Heiblum, M., Umansky, V. & Mahalu, D. Shot noise and charge at the $2/3$ composite fractional quantum Hall state. *Physical Review Letters* **103**, 236802 (2009).

Supplementary Note 1: Eliminating bulk thermal transport

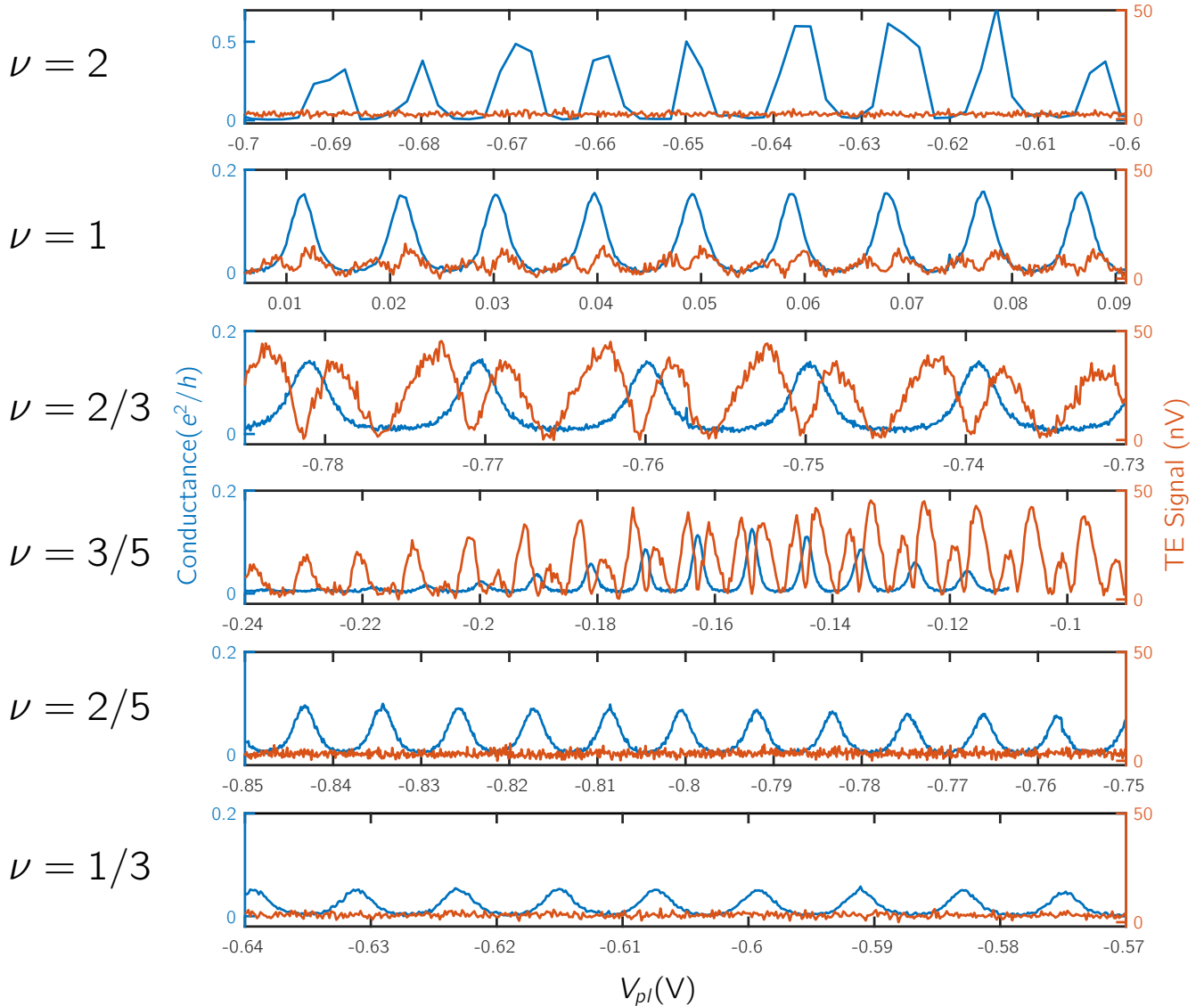
Here we present a second sample studied in order to probe if any contribution to the heat measured by the quantum dot was propagating through the bulk and not only through the edge modes. The device is very similar to the one from the main text. A deflector gate is placed before the quantum dot that allows to redirect the neutral modes to the ground directly. The results of the thermoelectric current measured versus the plunger gate voltage for the two configurations, deflector open and close, are presented on Supplementary Figure 1. When the QPC is closed a net thermoelectric current is measured similarly to the main paper sample. Nevertheless, one can notice that the thermoelectric current is only positive, which is due to the fact that we used a spectrum analyzer, only sensitive to the absolute value of the signal. Conversely, when the deflector is open, no thermoelectric current is measured by the quantum dot, which shows that no measurable contribution arise from the bulk.



Supplementary Figure 1. Measurement of the second sample: **a)** Configuration corresponding to the measurement of the Coulomb blockade peaks. both sides of the quantum dot are at base temperature. Sourcing current from S results in transmission peaks measured in D1 when changing the plunger gate voltage, as visible on **b)**. **c)** Configuration corresponding to the measurement of the neutral transmission using the thermoelectric current created through the quantum dot when the deflector gate is closed. **d)** Evolution of the thermoelectric current across the quantum dot as function of the plunger gate voltage. **e)** Configuration corresponding to the measurement of the neutral transmission using the thermoelectric current created through the quantum dot when the deflector gate is open **f)** No thermoelectric current is measurable through the QD when the deflector is open showing that no heat transport is happening in the bulk of the sample.

Supplementary Note 2: Upstream neutral modes at other filling factors

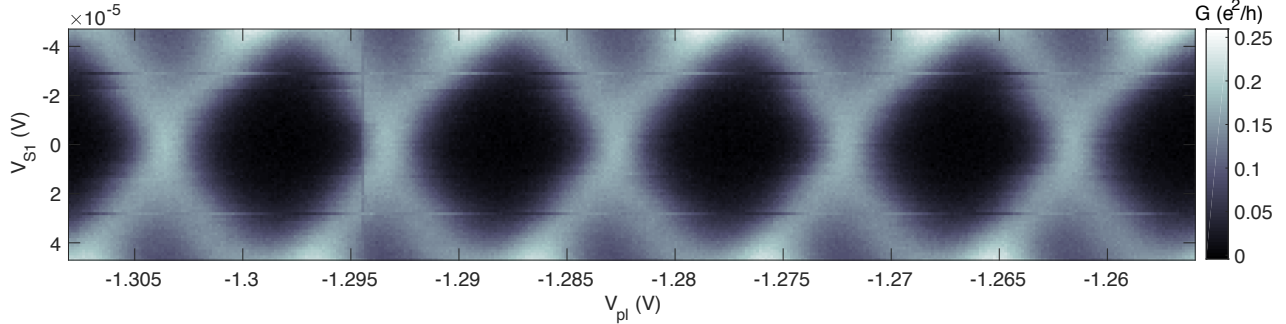
In Supplementary Figures 2 we present thermoelectric measurements at other filling factors, $\nu = 2, 1, 2/3, 3/5, 2/5, 1/3$ together with the coulomb blockade (CB) conductance as function of the plunger gate. At all of the measurements we sourced AC voltage of $V_H \sim 70 \mu V_{RMS}$ and scanned the plunger over a range of CB peaks where the QPC is fully open and the deflector gate is energized. At fillings $\nu = 2, 2/5$ and $1/3$ there were no measurable thermoelectric voltage, consisting with the lack of upstream neutral modes at these states. At fillings $\nu = 1, 2/3$ and $3/5$ we measure significant thermoelectric voltage consisting with the upstream neutral expected in the hole-conjugate states ($\nu = 2/3$ and $3/5$). At filling $\nu = 1$ upstream heat mode was measured before [1, 2] and it was attributed to a state of $\nu = 2/3$ underlying the $\nu = 1$.



Supplementary Figure 2. Evolution of the Coulomb peaks and thermoelectric currents for several filling factors: Thermoelectric voltage at other filling factors, $\nu = 2, 1, 2/3, 3/5, 2/5, 1/3$. Blue curves - left axes - conductance through the QD tuned to Coulomb blockade regime. Orange curves - right axes - thermoelectric voltage at the same regime. Measured with the deflector gate energized and $V_H \sim 70 \mu V_{RMS}$

Supplementary Note 3: Quantum Dot Coulomb diamonds

Here is presented the evolution of the conductance in the quantum dot as function of the voltage applied in S1 and the plunger gate. The extracted charging energy is $\sim 25 \mu\text{eV}$ which corresponds to an equivalent temperature of $\sim 290 \text{ mK}$.



Supplementary Figure 3. Coulomb Diamonds: Evolution of the conductance of the quantum dot as function of V_{S1} and V_{pl} . Coulomb diamonds are visible with a typical charging energy of $25 \mu\text{eV}$ with corresponds to an equivalent temperature of $\sim 290 \text{ mK}$

Supplementary Note 4: Theoretical model

Fractional quantum Hall states at simple Landau level filling fractions like $\nu = 1/m$ with odd m could be described by the Laughlin wave function [3]:

$$\langle z_1, \dots, z_n | \Psi_L \rangle \propto \prod_{i < j} (z_i - z_j)^m \exp\left[-\frac{1}{4l_B^2} \sum_i |z_i|^2\right], \quad (1)$$

where $z_i = x_i + iy_i$ are complex coordinates of electrons in the plane of two-dimensional electron gas and $l_B = \sqrt{\hbar c / eB}$ is the magnetic length. This state features fractionally charged anyons that are created by the operator $\psi^\dagger(\zeta)$ defined via

$$\langle z_1, \dots, z_n | \psi(\zeta) | \Psi_L \rangle = \prod_i (\zeta - z_i) \langle z_1, \dots, z_n | \Psi_L \rangle. \quad (2)$$

The Laughlin wave function (1) has a great success in describing various aspects of the corresponding fractional quantum Hall states. It has also been shown to be very close to exact eigenstate by numeric calculations and shown to be a universal exact wave function for short range interactions.

For more complex filling fractions like $\nu = 2/3, 3/5$, etc., it is still not completely clear what is the structure the wave function. Here we focus on the $\nu = 2/3$ state and discuss consequences for other filling factors later. There are two points of view on the $\nu = 2/3$ state. One considers this state as a charge conjugate to the $\nu = 1/3$ state. In other words, holes in the completely filled Landau level $\nu = 1$ form a Laughlin condensate with $\nu = 1/3$. Another one considers $\nu = 2/3$ state as a $\nu = 1$ type condensate of fractional $e^* = 1/3$ quasi-particles on top of the $\nu = 1/3$ state. It can be described by the wave function:

$$|\Psi_{\frac{2}{3}}\rangle \sim \int J(\zeta, \bar{\zeta}) d^M \zeta d^M \bar{\zeta} \prod_{i < j} (\zeta_i - \zeta_j) \exp\left[-\frac{1}{4ml_B^2} \sum_i |\zeta_i|^2\right] \prod_i \psi^\dagger(\zeta_i) | \Psi_L \rangle. \quad (3)$$

Note that the magnetic length of inner condensate is renormalized by \sqrt{m} . Such construction in general could describe various filling factors in the hierarchic manner [4].

We argue that the present experiment indicates that the second point of view is more appropriate. In order to investigate the edge structure of such state (3), we take into account that the energy scales are much lower than the fractional gap and use the effective low-energy theory [5, 6, 7] to describe the edge states. It has been shown [8] that the generic action for Abelian effective model of edge states can be always cast in the form:

$$S[\phi_s] = \frac{1}{4\pi} \sum_s \int dt dx [\sigma_s D_t \phi_s D_x \phi_s - v_s (D_x \phi_s)^2 + Q_s \epsilon^{\mu\nu} a_\mu \partial_\nu \phi_s], \quad (4)$$

where $\mu = x, t$, $\sigma_s = \pm 1$ denotes chirality of the corresponding eigenmode, and covariant derivative $D_\mu \phi_s = \partial_\mu \phi_s + \sigma_s Q_s a_\mu$ depends on the couplings Q_s of the corresponding modes to the external electro-magnetic potential a_μ . The charge density operator in such theory is expressed in terms of boson fields as $\rho_s = (\sigma_s Q_s / 2\pi) \partial_x \phi_s$. There has been proposed an edge reconstruction picture [14] as shown in Fig S3. Here we follow this idea and propose a particular model with $\hat{Q} = (1/\sqrt{3}, 1/\sqrt{3}, 0, 0)^T$, $\sum_s \sigma_s Q_s^2 = \nu$ and electron fields:

$$\phi_1 = \sqrt{3}\phi_c + \sqrt{\frac{3}{2}}\phi'_n + \frac{1}{\sqrt{2}}\phi''_n \quad (5a)$$

$$\phi_2 = \sqrt{3}\phi_c + \sqrt{2}\phi''_n \quad (5b)$$

$$\phi_3 = \sqrt{3}\phi_c - \sqrt{\frac{3}{2}}\phi'_n + \frac{1}{\sqrt{2}}\phi''_n \quad (5c)$$

Note that such model differs from proposed in Ref. [14] only in the degenerate subspace of the neutral modes. In the limit of strong interactions the velocity of charged mode is large $v_c \gg v'_n, v''_n$. We speculate that the width of inner reconstructed modes is also large $\xi/\xi_0 \gg 1$. This is consistent with the fact that the correlation length in the inner condensate of (3) is larger. Statistical phases for electronic excitation are indeed fermionic $\theta_{\alpha\beta} = \pi K_{\alpha\beta}$, $\alpha, \beta = 0, \dots, 3$.

$$\hat{K} = \begin{pmatrix} 3 & 0 & 0 & 0 \\ 0 & 1 & 2 & 4 \\ 0 & 2 & 1 & 2 \\ 0 & 4 & 2 & 1 \end{pmatrix} \quad (6)$$

so that electron vectors form an integral lattice that has a hexagonal projection on the neutral sector. Quasi-particles must have single-valued wave functions as, e.g., Laughlin quasi-particles (2) discussed above. In the effective model language this translates into integer statistical phases with respect to all electronic excitation. In other words, quasi-particles form a dual lattice:

$$\chi_n = \frac{n_0}{\sqrt{3}}\phi_0 + \frac{n_1 - n_2 + n_3}{\sqrt{3}}\phi_c + \frac{n_3 - n_1}{\sqrt{6}}\phi'_n + \frac{n_1 - 2n_2 + n_3}{\sqrt{2}}\phi''_n \quad (7)$$

The charges of the corresponding excitation are $e_n^* = (n_0 + n_1 - n_2 + n_3)/3$ and the scaling dimensions are given by:

$$\Delta_n = \frac{1}{3}n_0^3 + n_1^2 - \frac{1}{3}n_2^2 + n_3^2 + \frac{4}{3}n_1n_3 - \frac{8}{3}n_2(n_1 - n_2 + n_3). \quad (8)$$

It is interesting to investigate the most relevant particles content in the inner channel, we index them as $\chi_{n_1 n_2 n_3}$. There is one excitation with $e^* = 1/3$ and $\Delta = 1/3$ that is decoupled from neutral modes:

$$\chi_{111} = \frac{\phi_c}{\sqrt{3}} \quad (9)$$

also there are three ‘‘neutralons’’ with $e^* = 0$ and $\Delta = 2/3$:

$$\chi_{110}, \chi_{10-1}, \chi_{011} \quad (10)$$

and conjugate. Interestingly there are six quasi-particles with $e^* = 1/3$ and $\Delta = 1$ (free fermion scaling dimension):

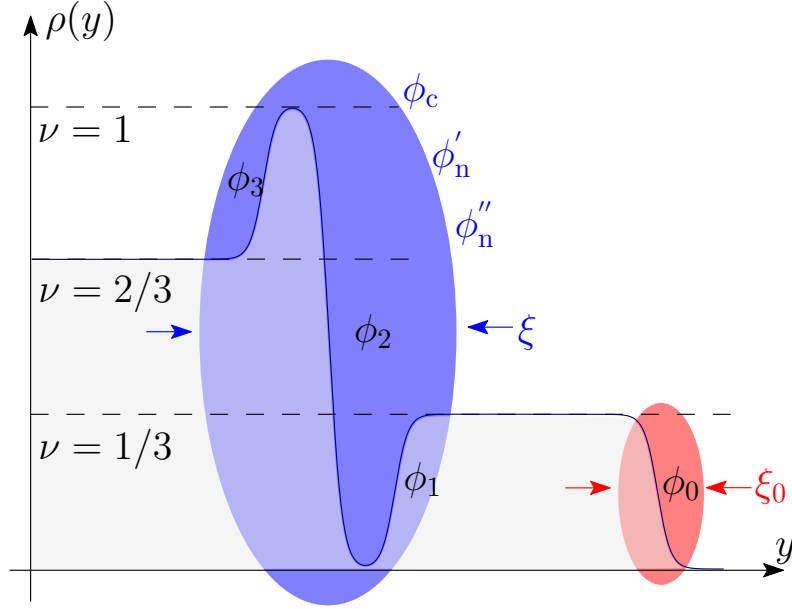
$$\chi_{001}, \chi_{100}, \chi_{012}, \chi_{210}, \chi_{122}, \chi_{221} \quad (11)$$

These could be a signature of $\nu = 1$ like condensate (plasmon waves on the boundary of inner condensate of $e^* = 1/3$ quasi-particles). These last quasi-particles (11) have non-zero charge and are coupled to the upstream modes. Therefore they are responsible for the dominant contribution to the thermo-electric effects upstream.

Quantitative results: Thermo-electric current

Upstream thermo-electric current through a single level with energy ϵ_0 can be estimated as

$$I_{\text{th-el}} \propto [f_D(\epsilon_0)f_U(-\epsilon_0) - f_U(\epsilon_0)f_D(-\epsilon_0)] \quad (12)$$



Supplementary Figure 4. Theoretical edge state structure: Schematic of the effective edge model. The blue curve shows possible transversal profile of charge density near the boundary of two-dimensional electron gas. In the effective theory, the inner modes are described in a universal way by three boson fields $\phi_c, \phi'_n, \phi''_n$ with action (4). Note that these modes have larger width than the outermost charged mode.

Here effective occupation numbers $f_i(\epsilon_0)$ are simply Fourier transforms of the corresponding correlation functions:

$$f(\epsilon_0) = \int dt e^{i\epsilon_0 t} K(t) \quad (13a)$$

$$K(t) = \langle \exp[-i\chi_n(t)] \exp[i\chi_n(0)] \rangle \quad (13b)$$

We take into account that downstream modes on the upper edge of quantum dot originate from a cold reservoir with base temperature T_0 , while upstream modes are from "hot" Ohmic contact with temperature T_1 . Assuming that the dominant cooling mechanism is by four edge states [9, 10], and taking into account that every chiral bosonic mode at temperature T carries a heat flux $\pi T^2/12$ we could write down the heat balance equation between the heat produced in the contact and heat dissipated (carried away by edge modes):

$$l\Delta\mu = \frac{\pi}{3} (T_1^2 - T_0^2). \quad (14)$$

Therefore we find that $T_1 = \sqrt{T_0^2 + (\Delta\mu/\pi)^2}$ for $\nu = 2/3$ and we have:

$$f_U(\epsilon_0) = \int dt e^{i\epsilon_0 t} \left[\frac{T_0}{\sinh(\pi T_0(t - i\eta))} \right]^{\delta_0} \left[\frac{T_1}{\sinh(\pi T_1(t - i\eta))} \right]^{\delta_1}. \quad (15)$$

In our model $\delta_0 = 1/3, \delta_1 = 2/3$ and $\Delta = \delta_0 + \delta_1 = 1$. For the lower edge effective occupation coincides with free fermions, since $\Delta = 1$:

$$f_D(\epsilon_0) = \int dt e^{i\epsilon_0 t} \frac{T_0}{\sinh(\pi T_0(t - i\eta))} = \frac{1}{e^{\epsilon_0/T} + 1} \quad (16)$$

We could also estimate the upper effective occupation (13) taking into account that at small energies the integral comes from the large times, where the correlation function decays exponentially:

$$K(t) \simeq \exp[-\pi T_{\text{eff}}|t|], \quad T_{\text{eff}} = \frac{T_0 + 2T_1}{3}. \quad (17)$$

Thus one could make an estimation:

$$f_U(\epsilon_0) \sim \frac{1}{e^{\epsilon_0/T_{\text{eff}}} + 1} \quad (18)$$

Results of this approximation as compared to exact numeric integration are shown in Fig 2d in the main text . They also agree well with the experimental data.

The asymptotic behavior of the thermo-electric current (12) in effective temperature approximation is

$$I_{\text{th-el}} \sim \Delta\mu^2/T_0^2, \quad \Delta\mu \ll T_0 \quad (19a)$$

$$I_{\text{th-el}} \sim \text{const}, \quad \Delta\mu \gg T_0 \quad (19b)$$

The saturation constant itself does not depend on base temperature T_0 when it is sufficiently low, but is suppressed as $\delta\epsilon_0/T_0$ when temperature becomes comparable with the level spacing $\delta\epsilon_0$ of the quantum dot.

Qualitative discussion: QPC charge and neutral transmissions

The key ingredient for the results of previous section is the electron-like scaling behavior of fractional quasi-particles (11). Here we also use the argument that the fractional quasi-particles coupled to neutral modes behave like free electrons. It is important to note that the effective action (4) is an intermediate fixed point, it has relevant neutralons $\Delta = 2/3$. In contrast, low-energy fixed point of Polchinski-Kane-Fisher model [11] has only irrelevant neutralons with $\Delta = 2$. However, quantum point contacts and quantum dots can give additional energy scale that pins the intermediate fixed point.

There are three wide inner states in our model: one charged and two upstream neutral and one narrow charged outer. The transmission of a single channel could be modeled in the quasi-classical approximation [12, 13] as

$$t_i(V) = \frac{1}{1 + e^{(V_i - V)/\delta V_i}} \quad (20)$$

where $i = \text{in, out}$. In our model there are two channels that are spatially separated, therefore they will be pinched off at different QPC voltages:

$$t_{\text{charge}}(V) = \frac{1}{2} \left[\frac{1}{1 + e^{(V_{\text{in}} - V)/\delta V_{\text{in}}}} + \frac{1}{1 + e^{(V_{\text{out}} - V)/\delta V_{\text{out}}}} \right] \quad (21)$$

Analogously, both neutral modes are located at inner channel, so that:

$$t_{\text{neutral}}(V) = \frac{1}{1 + e^{(V_{\text{in}} - V)/\delta V_{\text{in}}}} \quad (22)$$

It is natural to assume that $\delta V_{\text{in}}/\delta V_{\text{out}} \propto \xi/\xi_0 \gg 1$.

- Appearance of quasi-particles with charge $e^* = 1/3$ but with electronic scaling dimension $\Delta = 1$.
- Couplings of the above quasi-particles to the charged and neutral modes are universal $\delta_0 = 1/3$ and $\delta_1 = 2/3$ in the limit of strong Coulomb interactions.
- Inner and outer edge channels have significantly different widths $\xi/\xi_0 \gg 1$.
- Upstream neutral excitation only appear in the inner channel.

Most of these features will appear in all other filling fractions that allow hierarchic condensates. And indeed, the experimental data for $\nu = 3/5$ show that all the results are very similar.

Supplementary References

- [1] Vivek Venkatachalam, Sean Hart, Loren Pfeiffer, Ken West, and Amir Yacoby. Local thermometry of neutral modes on the quantum Hall edge. *Nature Physics*, 8(9):676–681, aug 2012.
- [2] Itamar Gurman, Ron Sabo, Moty Heiblum, Vladimir Umansky, and Diana Mahalu. Dephasing of an electronic two-path interferometer. *Physical Review B*, 93(12):121412, mar 2016.

- [3] R. B. Laughlin. Anomalous Quantum Hall Effect: An Incompressible Quantum Fluid with Fractionally Charged Excitations. *Physical Review Letters*, 50(18):1395–1398, may 1983.
- [4] S M Girvin R.E. Prange. See Chapter 7 in "The Quantum Hall Effect". *Springer, New York*, 93, 1987.
- [5] B I Halperin. Quantized Hall conductance, current-carrying edge states, and the existence of extended states in a two-dimensional disordered potential. *Physical Review B*, 25(4):2185–2190, 1982.
- [6] X. Wen. Chiral Luttinger liquid and the edge excitations in the fractional quantum Hall states. *Physical Review B*, 41(18):12838–12844, jun 1990.
- [7] J Frohlich and A Zee. Large scale physics of the quantum hall fluid. *Nuclear Physics B*, 364(3):517–540, 1991.
- [8] Ivan P Levkivskiy. Universal nonequilibrium states at the fractional quantum Hall edge. *Physical Review B*, 93(16), 2016.
- [9] So Takei and Bernd Rosenow. Neutral mode heat transport and fractional quantum Hall shot noise. *Physical Review B*, 84(23), 2011.
- [10] Artur O Slobodeniuk, Ivan P Levkivskiy, and Eugene V Sukhorukov. Equilibration of quantum Hall edge states by an Ohmic contact. *Physical Review B*, 88(16):165307, oct 2013.
- [11] C. L. Kane, Matthew P. A. Fisher, and J. Polchinski. Randomness at the edge: Theory of quantum Hall transport at filling $\nu=2/3$. *Physical Review Letters*, 72(26):4129–4132, jun 1994.
- [12] L D Landau and E M Lifshitz. Course of Theoretical Physics - Vol 3 Quantum Mechanics - nonrelativistic theory 3rd ed, 1977.
- [13] M Buttiker. Quantized transmission of a saddle-point constriction. *Physical Review B*, 41(11):7906–7909, 1990.
- [14] Wang, J., Meir, Y. & Gefen, Y. Edge reconstruction in the $\nu=2/3$ fractional quantum Hall state. *Physical review letters* 111, 246803 (2013).